Effects of strain and oxygen vacancies on the ferroelectric and antiferrodistortive distortions in PbTiO₃/SrTiO₃ superlattice

Menglei Li,[1,2] Jia Li,[3] Long-Qing Chen,[4,5] Bing-Lin Gu,[2,6] and Wenhui Duan[1,2,6,*]

[1]*Department of Physics and State Key Laboratory of Low-Dimensional Quantum Physics, Tsinghua University, Beijing 100084, People's Republic of China*

[2]*Collaborative Innovation Center of Quantum Matter, Tsinghua University, Beijing 100084, People's Republic of China*

[3]*Institute of Advanced Materials, Graduate School at Shenzhen, Tsinghua University, Shenzhen 518055, People's Republic of China*

[4]*Department of Materials Science and Engineering, Pennsylvania State University, University Park, Pennsylvania 16802, USA*

[5]*School of Materials Science and Engineering, Tsinghua University, Beijing 100084, People's Republic of China*

[6]*Institute for Advanced Study, Tsinghua University, Beijing 100084, People's Republic of China*

The effects of oxygen vacancy (V_O) and epitaxial strain on the ferroelectric (FE) and antiferrodistortive (AFD) properties of the [001]-oriented PbTiO₃/SrTiO₃ 1/1 superlattice are comprehensively studied using first-principles calculations. It is found that the oxygen vacancies form most easily when the superlattice in-plane lattice constant is between those of single-crystal PbTiO₃ and SrTiO₃. The polarization in the direction of the Ti-V_O-Ti chain is remarkably reduced due to the V_O-induced local tail-to-tail polarization patterns, and consequently, the V_O can pin the polarization to a certain direction. Moreover, the octahedral rotation or tilting around the direction of the Ti-V_O-Ti chain is also suppressed while the rotations along the other two orthogonal directions are enhanced. In both perfect and oxygen-deficient superlattices, the ferroelectric phase has lower energy when the octahedra rotate around the polar axis. These results suggest a promising way to mediate the FE and AFD properties in oxygen-deficient superlattices.

PACS number(s): 77.80.bn, 61.72.−y, 77.55.Px

I. INTRODUCTION

In recent years, ferroelectric-dielectric heterostructures have been the focus of experimental and theoretical attentions due to their polarization enhancement and other improved properties over single-component thin film [1,2]. Experimental techniques, including pulsed-laser deposition and radio-frequency magnetron sputtering, are well developed to grow high-quality ultrashort period oxide superlattices on certain substrates [3,4]. It is thus feasible to tailor the ferroelectric and dielectric properties in these artificial structures via various degrees of freedom, such as the composition ratio, substrate strain, etc. Among all methods, the epitaxial strain-mediated method realized by growing the superlattices on different substrates is particularly effective because of the strong coupling between polarization and strain.

In general, strain can induce changes in the in-plane metal-oxygen bond lengths and/or rigid rotation of the oxygen octahedra, resulting in the change of macroscopic polarization [5], which plays a critical role in the mediation of ferroelectricity. For BaTiO₃/SrTiO₃ superlattices, Neaton and Rabe [6] pointed out that the combination of strain effect and internal electric fields is responsible for the enhanced ferroelectricity. Recently, in 1/1 period superlattices of PbTiO₃/SrTiO₃ (PT/ST), Bousquet and co-workers showed an unexpected ground state combining both ferroelectric (FE) distortions and antiferrodistortive (AFD) rotations of the oxygen octahedra [7]. They demonstrated a novel kind of *improper ferroelectricity*, in which the octahedral rotations were the primary order parameter to drive the phase transition. Further, first-principles investigation indicated that the two distortions

strongly couple in (PbTiO₃)$_n$/(SrTiO₃)$_n$ superlattices when the periodicity $n < 3$ [8]. By symmetry analysis, Rondinelli and Fennie [9] proposed a design strategy that in layered perovskite superlattices $(ABO_3)_1/(A'B'O_3)_1$ composed of nonpolar compounds, the octahedral rotations in the parent single phases solely can introduce novel ferroelectricity.

On the other hand, oxygen vacancies are common but particularly important point defects in perovskite oxides and their heterostructures. It is known that in the growth of perovskite oxide films, heterostructures, and superlattices, the strain always exists, resulting in the nonstoichiometric accommodation of oxygen vacancies. Moreover, oxygen vacancy is the origin of many intriguing phenomena, such as two-dimensional electron gas at the interface of LaAlO₃/SrTiO₃ heterojunctions [10], ferromagnetism in strained epitaxial LaCoO₃ [11], reduction in free-carrier densities [12], and AFD-like oxygen octahedral rotation pattern in ST [13]. In particular, oxygen vacancies could be a major contributor to the fatigue and aging in conventional ferroelectrics PT by introducing tail-to-tail polarizations [14]. But in the multiferroic BiFeO₃, the ferroelectricity turns out to be independent of strain or oxygen vacancies [15]. As to the ferroelectric-dielectric superlattice, the effect of the oxygen vacancies on the *improper ferroelectricity* remains elusive due to the complexity of the system. Theoretical work on the oxygen-deficient perovskite superlattices is highly desired to provide guidance to the experiments and develop a new freedom of ferroelectricity modulation, combining with the strain. First-principles calculations, as a powerful theoretical tool, are widely performed to predict novel properties in the superlattices and explore the mechanism behind the experimental observations [6–8,16–24].

In this work, using first-principles calculations, we investigate the ferroelectric and antiferrodistortive distortions in

*dwh@phys.tsinghua.edu.cn

PT/ST 1/1 superlattice, a prototypical ferroelectric-dielectric superlattice, with different kinds of oxygen vacancies (V_O) under varied epitaxial strains. We find that when the strain is compressive for the PT layer while tensile for ST layer, the V_O formation energy is the lowest. Most kinds of V_O can pin the polarization to a certain direction in the superlattice by introducing tail-to-tail polarizations along the Ti-V_O-Ti chain which can cancel the total polarization, just as V_O in single-phase PT. V_O can also influence the oxygen octahedral rotations. Particularly, the octahedral rotations or tilts around the direction of the Ti-V_O-Ti chain are suppressed while those around other directions are enhanced. However, the coupling between the polarization and rotation (tilt) around the polar axis is not changed by the presence of V_O.

This paper is organized as follows. First, we describe the details of first-principles calculations as well as the configuration of the superlattices in Sec. II. In Sec. III we revisit the FE and AFD dependencies on epitaxial strain in vacancy-free PT/ST superlattice and compare our results with previous works. After that, in Sec. IV, we investigate different kinds of oxygen vacancies in the most stable phase of the superlattice, calculating the formation energies, electric polarizations, and specific oxygen octahedral rotation and tilt angles. Then we discuss the physical mechanism of ferroelectric and antiferrodistortive distortions in Sec. V. Lastly, we give a brief summary in Sec. VI.

II. METHODOLOGY

We perform first-principles calculations within density functional theory (DFT) as implemented in the *Vienna Ab initio Simulation Package* (VASP) [25]. The projector augmented wave pseudopotentials [26] are employed within the local density approximation (LDA) [27]. Ba $5s$, $5p$ and $6s$ electrons; Sr $4s$, $4p$, and $5s$ electrons; Ti $3s$, $3p$, $3d$, and $4s$ electrons; and O $2s$ and $2p$ electrons are treated as valence electrons. We expand electronic wave functions in plane waves using an energy cutoff of 520 eV. The structural relaxations are carried out with the conjugate gradient algorithm [28] until the residual forces are less than 0.01 eV/Å. The $7 \times 7 \times 5$ Monkhorst-Pack k mesh is used for in-plane $\sqrt{2} \times \sqrt{2}$ enlarged supercells, while $3 \times 3 \times 3$ Monkhorst-Pack k mesh is for $2\sqrt{2} \times 2\sqrt{2}$ supercells. The formation energies of oxygen vacancies are calculated by using the formula $E_{form} = E_{V_O} + \mu(O) - E_{perfect}$, where $\mu(O)$ is half of the total energy of an O_2 molecule, $E_{perfect}$ and E_{V_O} are the total energies of the pristine superlattice and the superlattice with oxygen vacancy, respectively. It is known that a neutral V_O returns two electrons to d orbitals of Ti atoms. The spin-up and spin-down states, however, are equally occupied, and no magnetization arises, as demonstrated by our spin-polarized DFT calculations (shown in Fig. S2 of the Supplemental Material [29]). This reveals that the d electrons can be treated normally within the conventional LDA framework. Actually, it is a common way to deal with oxygen-deficient single-phase SrTiO$_3$ or PbTiO$_3$ [30–32].

The total polarization of the perfect superlattice can be calculated either with the Berry phase method [33] or the method proposed by Meyer and Vanderbilt [34]. With the latter method, the local cell-by-cell polarizations are first achieved by summing the products of Born effective charges (calcu-lated from the density functional perturbation theory [35]) and ion displacements in the local Pb- or Sr-centered unit cells. The average of the cell-by-cell polarizations is the total polarization, which is fairly close to the polarization calculated from Berry phase method (with a difference less than 2 μC/cm^2). Unfortunately, for the most oxygen-deficient systems, the Berry phase formalism and the Born effective charge calculation fail because the band structure could be metallic (see the Supplemental Material [29]). However, in practical ferroelectrics the polarization still exists though there are inevitably oxygen vacancies. The ion displacements, rather than the polarization, is often used to simulate this situation [36,37]. In order to give a primary estimation of the polarization in the defected superlattice, we still use the products of Born effective charges from the perfect superlattice and ionic displacements, providing that ions close to the vacancies are mostly screened by vacancy-induced carriers and their Born effective charges vanish while the ions at further distances can suffer less significant impacts. Although layer-decomposed electronic density of states analysis shows that the PbO layer and SrO layer are insulating (see the Supplemental Material [29]), the polarization is better estimated in unit-cell layers instead of single-atom layers because the sum of Born effective charges in a single-atom layer does not necessarily vanish [38]. Therefore, our adopted method of polarization calculation in an oxygen-deficient superlattice can to some extent avoid the issue of vacancy-induced metallicity and give a qualitatively reasonable evaluation of the polarizations.

To explore the FE and AFD distortions of the PT/ST superlattice, it is useful to first determine the ground states of bulk ST and PT at 0 K, separately. The bulk ST crystallizes in the nonpolar *I4/mcm* space group and has the $a^0 a^0 c^-$ AFD pattern in Glazer's notation [39] with the rotation angle of 6°. The ground state of bulk PT is the *P4mm* ferroelectric phase, with a polarization of 75.68 μC/cm^2 along the c axis as we computed. The calculated in-plane parameters of PT and ST are 3.894 Å (a_{PT}) and 3.863 Å (a_{ST}), respectively, slightly less than experimental values [18]. The PT/ST superlattices are constructed by alternately stacking layers of PT and ST along the pseudocubic [001] direction (also denoted as the c axis for simplification) as shown in Fig. 1. When biaxial strain is applied, the strain values ε for ST and PT layers are defined as $\varepsilon^{ST} = (a_{IP} - a_{ST})/a_{ST}$ and $\varepsilon^{PT} = (a_{IP} - a_{PT})/a_{PT}$, respectively, where a_{IP} is the in-plane lattice parameter imposed on the superlattice, and a_{PT} and a_{ST} are calculated equilibrium in-plane lattice parameters of the bulk PT and ST, respectively. During the geometry optimization, a_{IP} is fixed while the out-of-plane lattice parameter is relaxed.

Due to the possible instabilities of FE and AFD distortions, different initial states with symmetry-restricted optimization of superlattice are used for comparison of energies. The considered distortions include the FE instability at the Γ point in the Brillouin zone and several AFD modes at the M point of the Brillouin-zone boundary. Using Glazer's notation [39], these AFD modes are characterized by the octahedral rotation pseudocubic axes (a, b, or c) and relative rotations between the adjacent octahedra (the superscripts $+$ and $-$ represent, respectively, the rotations in the same ($+$) and opposite ($-$) directions; the superscript 0 represents no rotation). Due to the symmetry, the pseudocubic [100]
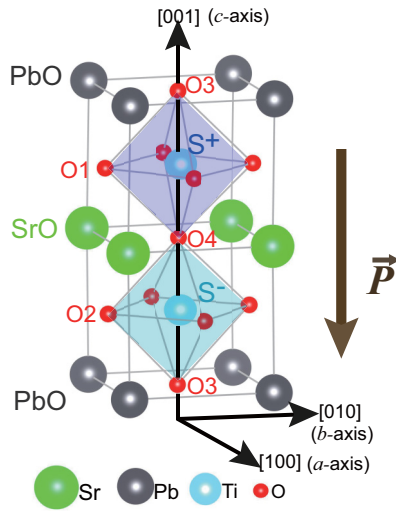
FIG. 1. (Color online) Schematic view of the PbTiO$_3$/SrTiO$_3$ 1/1 superlattice with FE and AFD distortions. The spontaneous polarization points down. The four kinds of oxygen atoms and the upper-layer octahedra (S$^+$) and the lower-layer octahedra (S$^-$) are denoted.

direction (*a* axis for simplification) and [010] direction (*b* axis for simplification) are equal. The resultant in-plane octahedral tilting axis and in-plane polarization direction are both along the [110] direction, which requires a $\sqrt{2} \times \sqrt{2} \times 1$ supercell of the PT/ST superlattice to consider AFD distortions.

For V_O, four types of inequivalent oxygen sites are considered, as shown in Fig. 1. The O atoms in the TiO layer are denoted as O1 and O2, while in the PbO layer and SrO layer they are denoted as O3 and O4, respectively. According to Fig. 1, the oxygen octahedra are indicated as S$^+$ (above the SrO plane) and S$^-$ (below the SrO plane), which are distinguishable in the superlattices with nonzero polarization along the *c* axis. To avoid the interaction between V_O and its periodic images, a $2\sqrt{2} \times 2\sqrt{2} \times 1$ supercell of the PT/ST superlattice is used with a distance of 8 Å from the V_O to its nearest image.

It should be noted that the concentration of the vacancies in the enlarged superlattice concerned is $\sim 2.1\%$, much higher than typical experimental values of 10^{-4}–10^{-5} under normal conditions [40]. Due to the huge computational cost, nowadays it is still very difficult to exactly reproduce the usual experimental defect concentration in the supercell DFT calculations, and smaller supercells of less than 100 atoms are generally adopted in the DFT calculations of vacancy systems [14,15,41]. According to the works of Evarestov *et al.* [42,43], the electronic structure, formation energy, lattice relaxation, migration energy, etc., are all dependent on the size of the supercell to varying degrees. On the other hand, many physical effects induced by vacancy defects are quite localized. Typically, the vacancy-induced atomic displacement between supercells of different sizes is around 10% [43] in bulk ST, which would not result in qualitative change in polarization and AFD distortions. This indicates that a reasonable evaluation of the oxygen vacancy effect on epitaxial strained superlattice can be obtained using the relatively smaller supercell and higher vacancy concentration.

III. COUPLING BETWEEN FE AND AFD INSTABILITIES IN PERFECT PT/ST SUPERLATTICE

The total energies of pristine superlattices with different symmetries against varying epitaxial strain are used to map out the strain phase diagram. When in-plane lattice parameter a_{IP} is between a_{PT} and a_{ST}, several phases are nearly equally stable with the energy difference less than 20 meV per supercell, consistent with the results from Bousquet *et al.* [7]. Among possible phases, four most stable phases are chosen to calculate the total energy over a wide range of strain for the strain phase diagram. The four considered phases are (1) the structure possessing an out-of-plane polarization with AFD rotations around the out-of-plane axis (FE$_c$/AFD$_c$, *P4bm*); (2) in-plane polarization with AFD tilts around the in-plane axis (FE$_{aa}$/AFD$_{aa}$, *Pmc2$_1$*); (3) both in-plane and out-of-plane polarizations with AFD rotations around both in-plane and out-of-plane axes (FE$_r$/AFD$_{aac}$, *Pc*), which has the lowest symmetry; and (4) in-plane polarization and AFD rotations around the out-of-plane axis (FE$_{aa}$/AFD$_c$, *Pnc2*). The last phase has higher energy than the other three phases at most considered strain regions and is only included for comparison.

It is clear from Fig. 2(a) that the FE$_r$/AFD$_{aac}$ phase is the ground state over the entire range of strain we studied. This phase was previously found in the BaTiO$_3$/CaTiO$_3$ superlattices, where the ground state is also predicted to have the *Pc* symmetry [44]. However, the FE$_r$/AFD$_{aac}$ phase is not prominently stressed by Bousquet *et al.*[7], because its total energy is close to those of FE$_c$/AFD$_c$ phase at compressive strain and FE$_{aa}$/AFD$_{aa}$ phase at tensile strain. Nevertheless, in PT/ST superlattice, the FE$_r$/AFD$_{aac}$ phase should be distinguishable from the FE$_c$/AFD$_c$ and FE$_{aa}$/AFD$_{aa}$ phases because the polarization dependence on strain is different for these three phases, as shown in Fig. 2(b). At intermediate strain (the area covered with a light-colored strip in Fig. 2(b)], the FE$_r$/AFD$_{aac}$ phase has both the in-plane and out-of-plane polarizations just as the so-called *r* phase found in ferroelectric thin films [45,46]. Moreover, under large compressive strain [i.e., the left part of Fig. 2(b)], the in-plane polarization vanishes; while under large tensile strain [i.e., the right part of Fig. 2(b)], the out-of-plane polarization vanishes. This overall polarization dependence on strain for the FE$_r$/AFD$_{aac}$ phase agrees well with that in PT/ST 2/2 superlattice predicted by Aguado-Puente *et al.* [8]. In contrast, along with increasing in-plane strain, the FE$_c$/AFD$_c$ phase only has monotonically decreasing out-of-plane polarization, while the FE$_{aa}$/AFD$_{aa}$ phase only has monotonically increasing in-plane polarization; in both phases, the polarization direction does not change upon strain. Interestingly, only the FE$_{aa}$/AFD$_c$ structure, the least stable phase among the four phases considered [as shown in Fig. 2(a)], exhibits the in-plane polarization and octahedral rotation around the out-of-plane axis, suggesting that the energy of the superlattice is lower when the polarization and the AFD rotation around the same polar axis coexist in the FE-AFD coupling regime. It is thus that the detailed properties of the FE$_{aa}$/AFD$_c$ structure will not be presented in the following.

For compressive strains, the octahedral rotation around the out-of-plane axis is unambiguously promoted, as shown in Fig. 2(c). Three most stable phases all have spontaneous
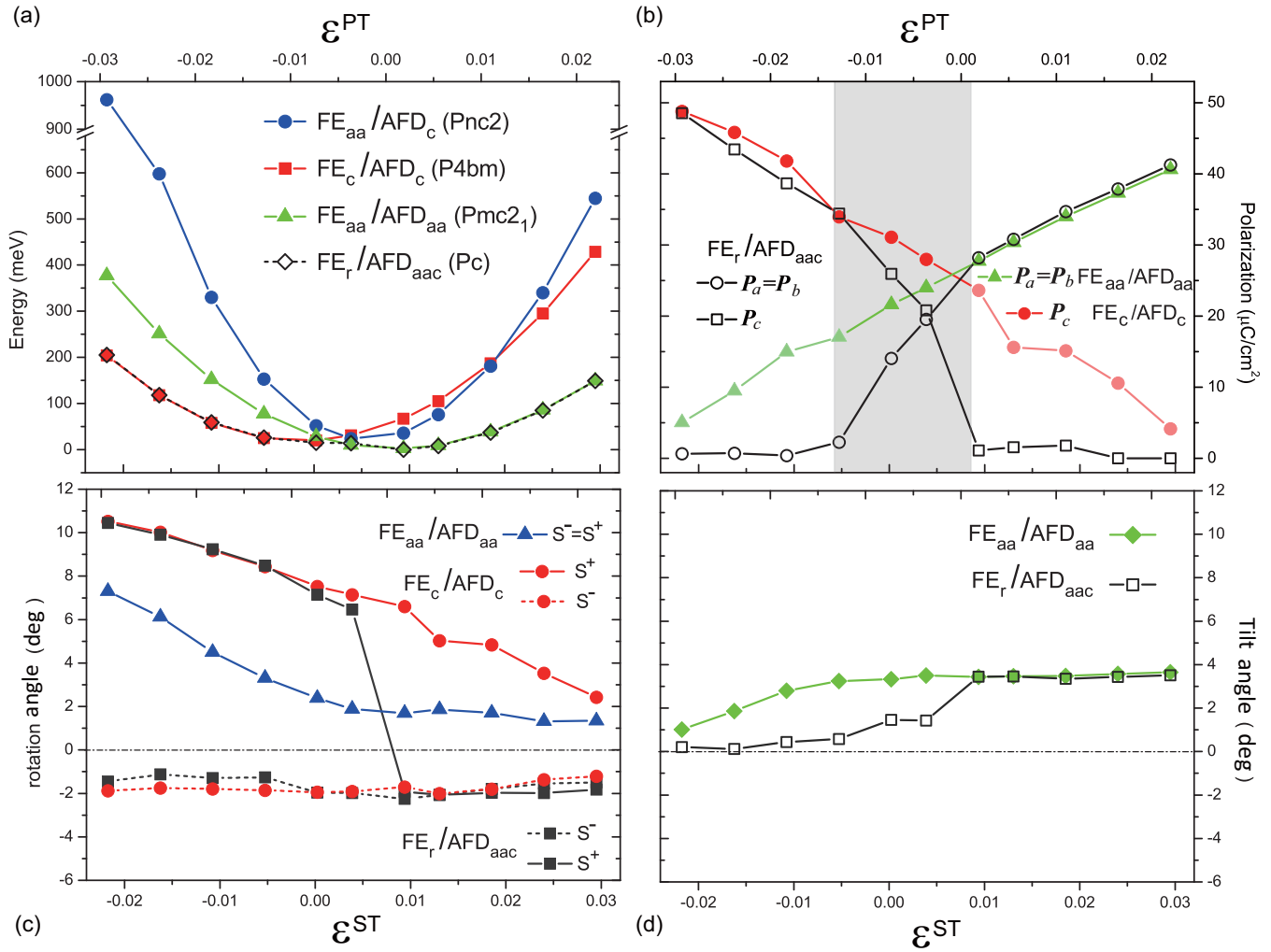
FIG. 2. (Color online) (a) Relative energies, (b) polarizations, (c) octahedral rotations around the out-of-plane axis, and (d) octahedral tiltings about in-plane axis of different phases in terms of epitaxial strains. In (b) P_a (P_b) is the in-plane polarization projection on the [100] ([010]) direction and $\mid P_a \mid = \mid P_b \mid$. The FE_{aa}/AFD_{aa} phase does not have the out-of-plane polarization (P_c) and the FE_c/AFD_c phase does not have the in-plane polarization (P_a and P_b). In (c) the rotation of S^+ is defined to be positive, and the positive (negative) angle of S^- rotation indicates that S^- rotates in the same (opposite) direction with S^+. Note that in the FE_{aa}/AFD_{aa} phase the S^- and S^+ have same rotations along the c axis. In (d) the angles of the in-plane tilts about the [100] and [010] axes completely coincide and thus represented by the same line.

octahedral rotations around the c axis, although the initial rotation pattern of $a^- a^- c^0$ for the FE_{aa}/AFD_{aa} phase does not include such out-of-plane rotation before relaxation. For the FE_r/AFD_{aac} phase, the upper-layer octahedra (S^+) and the lower-layer octahedra (S^-) have different rotations both in direction and in magnitude, consistent with previous works [7,8]. Aguado-Puente *et al.* ascribed this phenomenon to the imbalance between Pb-O and Sr-O covalent interactions. However, in PT/ST 1/1 superlattice, the mirror symmetry about the PbO (SrO) (001) plane is conserved. Thus, S^+ and S^- are originally equivalent and have the same chemical environment in the undistorted structure. The main reason behind different octahedral rotation angles is the existence of the nonzero out-of-plane polarization, resulting in breaking of the mirror symmetry about the PbO (SrO) (001) plane. For phases with sizable polarization along the c axis, such as the FE_c/AFD_c phase and the FE_r/AFD_{aac} phase at compressive strain, S^+ has different rotations from S^-. By contrast, for

phases with zero or small out-of-plane polarization, i.e., the FE_r/AFD_{aac} phase at tensile strain (out-of-plane polarization is smaller than 2 $\mu C/cm^2$) and the FE_{aa}/AFD_{aa} phase, the discrepancy between S^+ and S^- rotations will disappear. Therefore, the out-of-plane polarization is the key factor for the nonequal rotations of the upper and lower octahedra. Moreover, when the direction of the out-of-plane polarization is reversed, the rotations of S^+ and S^- are found to exchange their absolute values, indicating that the direction of the polarization along the c axis is also crucial.

Remarkably, the situation for tensile strains is different: octahedral tilting about the in-plane axis is dominant as shown in Fig. 2(d). Since the tilts about the [100] and [010] directions are of the same amplitude, the octahedra are projected onto the (110) plane to clearly show the $a^- a^- c$ AFD pattern [see Fig. 3(a)]. When tensile strain is applied, the contraction of the c axis is accommodated by a bending of the Ti-O-Ti chain along the c axis, resulting in the in-plane tilt pattern
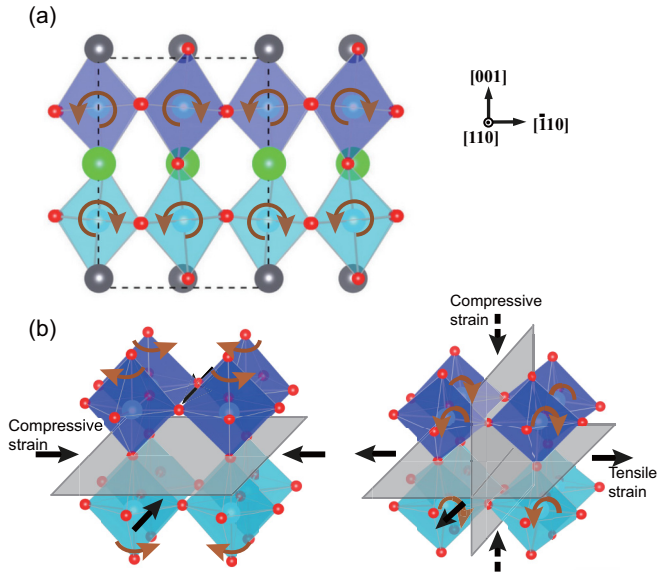
FIG. 3. (Color online) (a) The octahedral tilting about the in-plane [110] direction. Dashed line indicates the supercell boundary. (b) A schematic plot of how tensile strain induces the in-plane octahedral tilting as an analogy with the way compressive strain promotes the rotations around the out-of-plane axis.

through rigid rotations of the oxygen octahedra, as shown in Fig. 3(b). The close correlation between the polarization and AFD rotations will be discussed in Sec. V.

IV. THE ROLE OF OXYGEN VACANCY

Oxygen vacancies are a common point defect in perovskite oxides when strain is applied. In this section, we will investigate the effect of oxygen vacancies on the polarization and octahedral rotation (tilting) in the PT/ST superlattice with varying strain. If not stated otherwise, the FE_r/AFD_{aac} phase, which is the most stable structure of the PT/ST superlattice, is taken into account using a $2\sqrt{2} \times 2\sqrt{2} \times 1$ supercell.

A. Formation energy

A key question to be addressed is how the relative stability of different oxygen vacancies changes with varying strain. Figure 4(a) shows the formation energies of different V_O configurations as a function of the epitaxial strain. Although there is no literature on the formation energies of oxygen vacancies in PT/ST superlattices, previous theoretical studies have given some hints on the energy scales in bulk ST and PT. Under an extremely O-rich environment, the formation energy of charge-neutral oxygen vacancy in bulk ST is about 6 eV by hybrid density functional (HSE) [47] and 6.5 eV by LDA [41]. In bulk PT, V_O at different sites has the formation energy varying from 5.53 to 5.85 eV by LDA [48]. Our calculated formation energies of oxygen vacancies in PT/ST superlattices are in the range from 4.99 to 5.69 eV, less than those in single-phase bulk materials. Therefore, we expect that V_O forms more easily in the PT/ST superlattice than in the corresponding ST or PT bulk materials. Moreover, it is clear from Fig. 4(a) that the formation energies of V_{O1}, V_{O2},
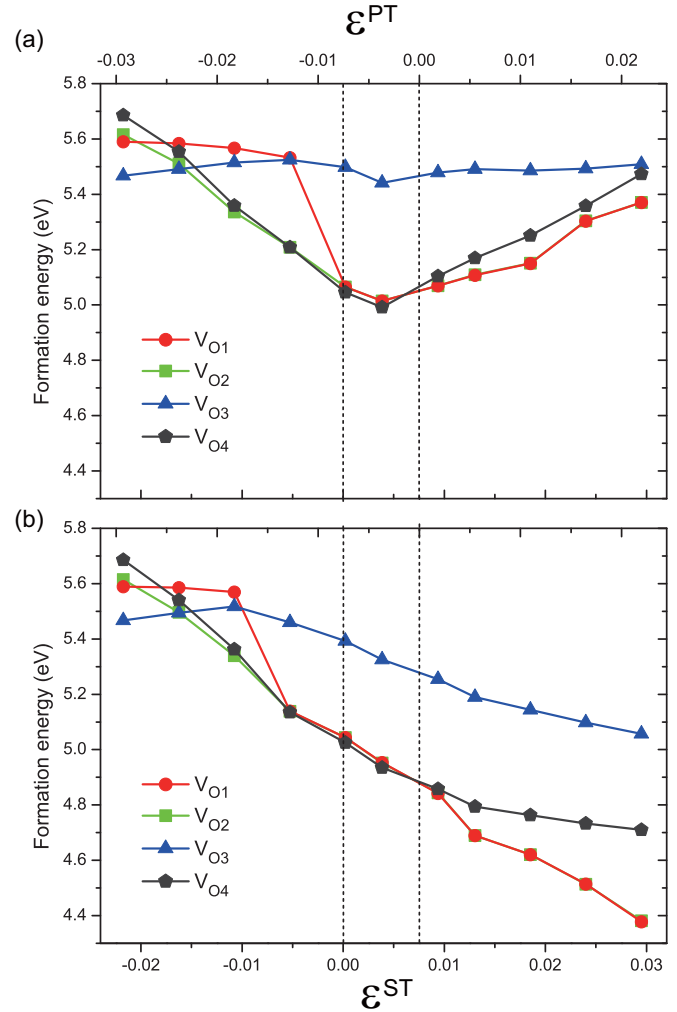

FIG. 4. (Color online) The formation energies of four kinds of oxygen vacancies in the (a) FE_r/AFD_{aac} and (b) FE_c/AFD_c phases as a function of epitaxial strains

and V_{O4} have the same trend, decreasing first, then increasing and reaching minima at the intermediate strain (i.e., $\varepsilon^{PT} < 0$ but $\varepsilon^{ST} > 0$). In contrast, the formation energy of V_{O3} nearly remains unchanged with varying epitaxial strain, and is higher than those of the other three V_O configurations when a_{IP} ranges from 3.84 Å to the maximum value considered here.

The polarization-induced internal electric field can be responsible for the relative stability of oxygen vacancies with varying strain. For PT/ST superlattices without oxygen vacancies, the total polarization first decreases and then increases with the increase of a_{IP} as shown in Fig. 2(b), resulting in the same trend of the internal electric field strength. For this reason, the introduction of oxygen vacancies should overcome higher electrostatic potential at high compressive and tensile strains than at intermediate strain. To support the above argument, we further calculate formation energies of V_O in the FE_c/AFD_c phase. The formation energies of all oxygen vacancies indeed decrease monotonically with the increase of strain [Fig. 4(b)], while the corresponding polarization of the perfect FE_c/AFD_c phase also decreases all the way as in Fig. 2(b). These results in turn show that
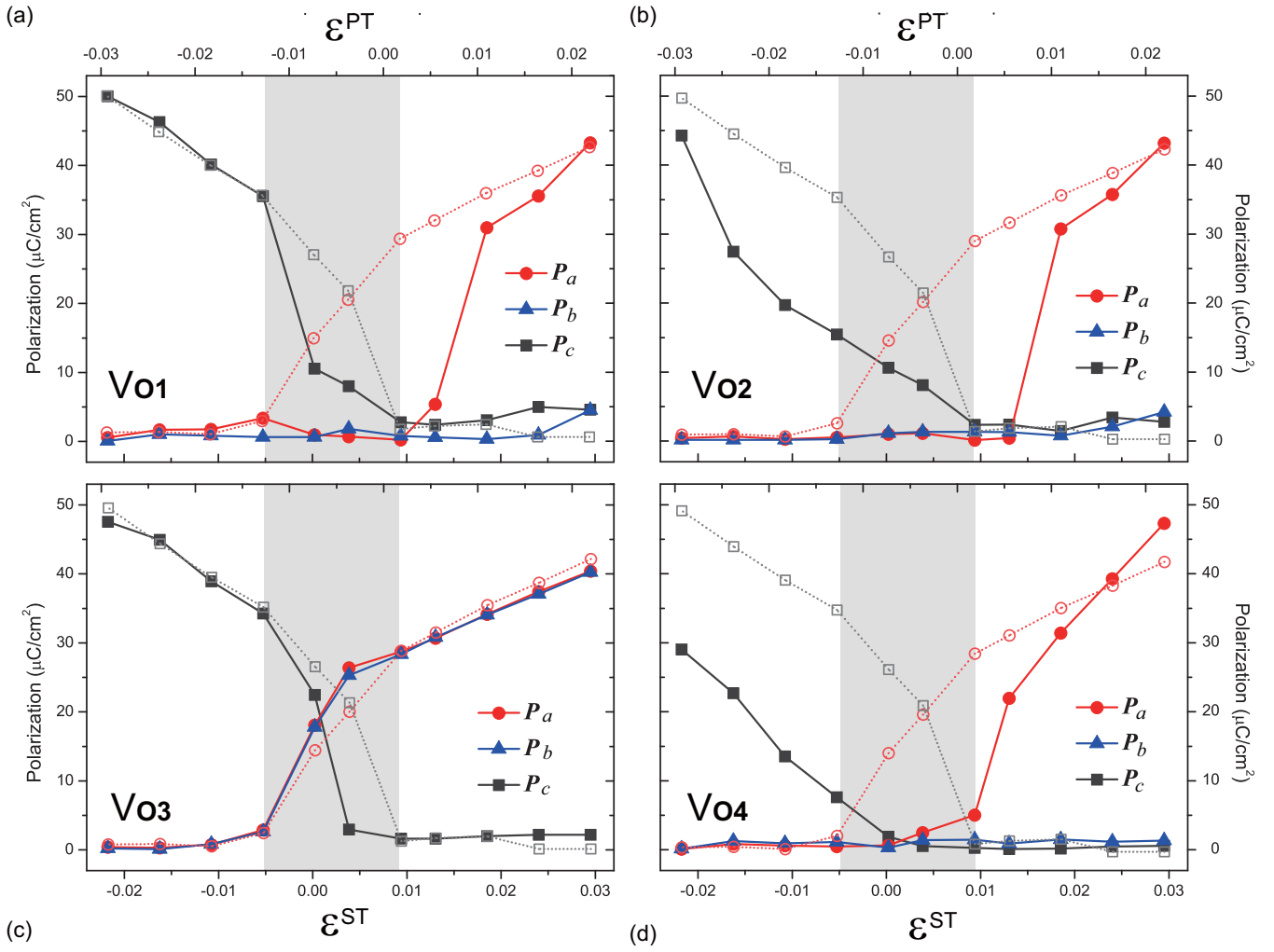
FIG. 5. (Color online) Average polarization vs epitaxial strain for the superlattices with (a) V_{O1}, (b) V_{O2}, (c) V_{O3}, and (d) V_{O4}. The dashed lines with hollow symbols indicate the polarization of the perfect SL. The light-colored ribbon indicates the range of strain at which the perfect SL has both in-plane and out-of-plane polarization components.

the polarization-induced internal electric field is responsible for the behavior of formation energy in the oxygen-deficient FE_r/AFD_{aac} phase. It should be noted that the formation energy of V_{O3} in the FE_r/AFD_{aac} phase exhibits exceptional strain dependence. The electronic structure analyses show that V_{O3} induces different changes in the density of states from other V_O (see the Supplemental Material [29]). The difference between V_{O3} and other V_O configurations will be further discussed in the following sections. Moreover, under intermediate strains, V_{O3} is less stable than the other three configurations by about 0.43 eV [see Fig. 4(a)], suggesting that even at 1000 K out of 100 oxygen vacancies only one is V_{O3}, as estimated from $e^{-\Delta H/kT}$ (ΔH is the defect formation energy) [49]. Evidently, this kind of oxygen vacancy (i.e., V_{O3}) is hardly formed in the PT/ST superlattice in comparison with the other three oxygen vacancies.

B. Polarization

Figure 5 shows the dependence of the polarization on epitaxial strain in oxygen-deficient PT/ST superlattices with four types of V_O. The polarization profiles of superlattices with V_{O1},

V_{O2}, and V_{O4} have two major features in common, remarkably different from the polarization variation in the defect-free superlattice. One feature is that the in-plane polarization is along the [100] direction instead of the [110] direction, together with a decrease in magnitude. Another feature is that at intermediate strain (the area covered with a light-colored strip in Fig. 5), the coexistence of in-plane and out-of-plane polarization (denoted as r phase) disappears. Specifically, the polarization direction of superlattice with V_{O4} is either in plane or out of plane, while for V_{O1} or V_{O2} only polarization along the [001] direction is left. However, for superlattice with V_{O3}, the polarization remains nearly unchanged compared to those of the perfect PT/ST superlattice. This is probably due to the insulating nature of the superlattice with V_{O3} under intermediate strain to tensile strain. According to the calculated electronic density of states (as shown in Figs. S3 and S4 of the Supplemental Material [29]), the superlattices with other kinds of V_O are metallic with the Fermi level crossing the conduction bands, and thus ferroelectricity deteriorates. On the contrary, the superlattice with V_{O3} is insulating: the two excess electrons induced by the neutral V_O occupy the impurity states which do *not* cross the Fermi level. Therefore,
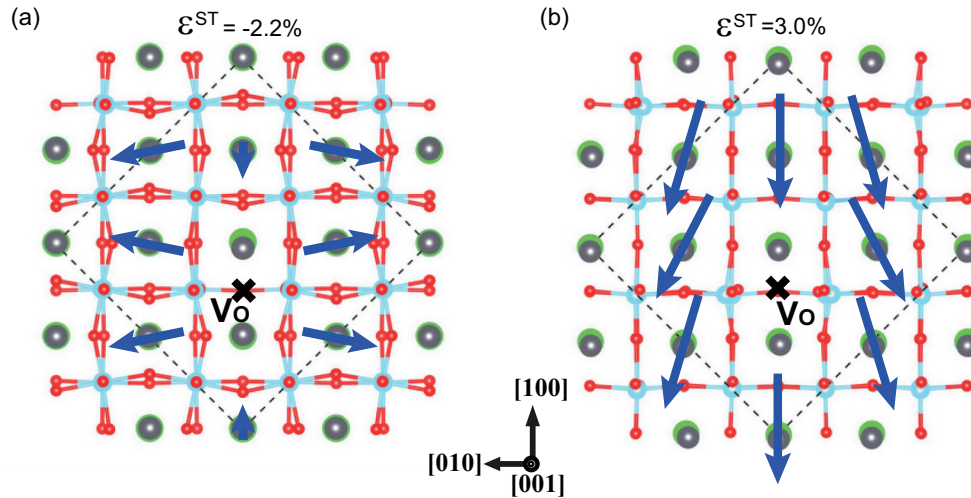
FIG. 6. (Color online) Schematic plot of the local polarization patterns for V_{O1} configuration under (a) compressive strain and (b) tensile strain. The supercell boundary is denoted by dashed lines. The direction and length of the arrow represent the direction and relative magnitude of local polarization, respectively. The longest arrow in (a) corresponds to a polarization of about 10 μC/cm^2 and that in (b) corresponds to about 40 μC/cm^2.

the ferroelectricity of the superlattice with V_{O3} could be well preserved.

At intermediate strain, the PT layer is squeezed while the ST layer is stretched; accordingly both out-of-plane and in-plane polarizations coexist in perfect PT/ST superlattices. The introduction of V_O can release the strain imbalance to some extent, reducing the total of tensile effect and compressive effect. Since the PT layer, the origin of the ferroelectricity in the superlattice, has the spontaneous out-of-plane polarization (i.e., [001] polarization) under this range of strain, the oxygen vacancy can partly recover the [001]-oriented ferroelectricity originated from the PT layer. Therefore, the intermediate-strain-induced polarization deviations from the out-of-plane axis are either eliminated as in superlattices with V_{O1} and V_{O2} [see Figs. 5(a) and 5(b)], or strongly attenuated together with the reduction of the [001] polarization itself as in superlattice with V_{O4} [see Fig. 5(d)], resulting in the disappearance of the coexistence of the in-plane and out-of-plane polarizations. This behavior is in agreement with the well-known vacancy pinning effect on the polarization switching, which contributes a lot to the fatigue in ferroelectrics [50–52]. Moreover, both the in-plane and out-of-plane polarizations are less than the polarizations in perfect superlattice as shown in Fig. 5, corroborating a negative effect of V_O on the ferroelectricity of the system. The out-of-plane polarization of superlattice with V_{O4} is smaller and vanishes faster than those with V_{O1} or V_{O2}. This can be explained from the anisotropic Born effective charge tensor of O atoms in ABO_3 compounds [53,54]. The Born effective charge in the [001] direction for O4 ($-5.9e$) is larger than those for O1 and O2 ($-2.1e$). Therefore, the removal of O4 would be more detrimental than O1 or O2 to the out-of-plane polarization. On the contrary, the in-plane polarizations of superlattice with V_{O1} or V_{O2} are less than those of superlattice with V_{O4} because the in-plane Born effective charge components for O1 and O2 are larger than those for O4.

As shown in Fig. 5, the polarization component along the in-plane [010] direction is negligibly small for the lowest-energy

configurations of V_{O1} and V_{O2}. This can be mainly attributed to the orientation of the Ti-V_O-Ti chain. In superlattices with V_{O1} or V_{O2}, the adjacent two Ti cations near the vacancy in the TiO layer move directly away from each other due to Coulomb repulsion. These atomic displacements lead to a tail-to-tail local polarization pattern along the Ti-V_O-Ti chain, which is approximately [010] oriented in our system. Thus, the total polarization in the [010] direction is suppressed, with only the [100]-direction polarization left. The appearance of this tail-to-tail pattern is independent of the strain. For illustration, the local polarization distributions under compressive and tensile strains are schematically plotted in Figs. 6(a) and 6(b), respectively. Because the oxygen vacancies tend to order into a chain or even planar structures [50], polarizations parallel to the direction of the vacancy chain will be significantly weakened. We therefore proposed that the ordering of oxygen vacancies can be used to block the polarization in unwanted directions.

C. AFD rotations

Now we turn to the octahedral rotation and tilt patterns in the defective superlattice. In the perfect superlattice, the oxygen octahedra have both the rotations around the [001] axis and the tilt about the in-plane axis (i.e., the rotations around the [110] direction). With oxygen vacancies, the tilt patterns become more complicated since the equivalence of the [100] and [010] directions can be destroyed. Consequently the octahedral rotation angles around the [100] (a axis), [010] (b axis), and [001] (c axis) directions are independent and possibly different now. Therefore, the changes of rotations around the out-of-plane axis (c axis) and tilts about in-plane axes will be separately discussed in the following.

Figure 7 shows the rotation angles around the c axis in oxygen-deficient superlattices under different epitaxial strains. Interestingly, the V_O-induced changes of the rotations exhibit different behaviors across $\varepsilon^{PT} = 0$. Under large compressive strain ($\varepsilon^{ST} < -0.01$), the rotations in all four V_O
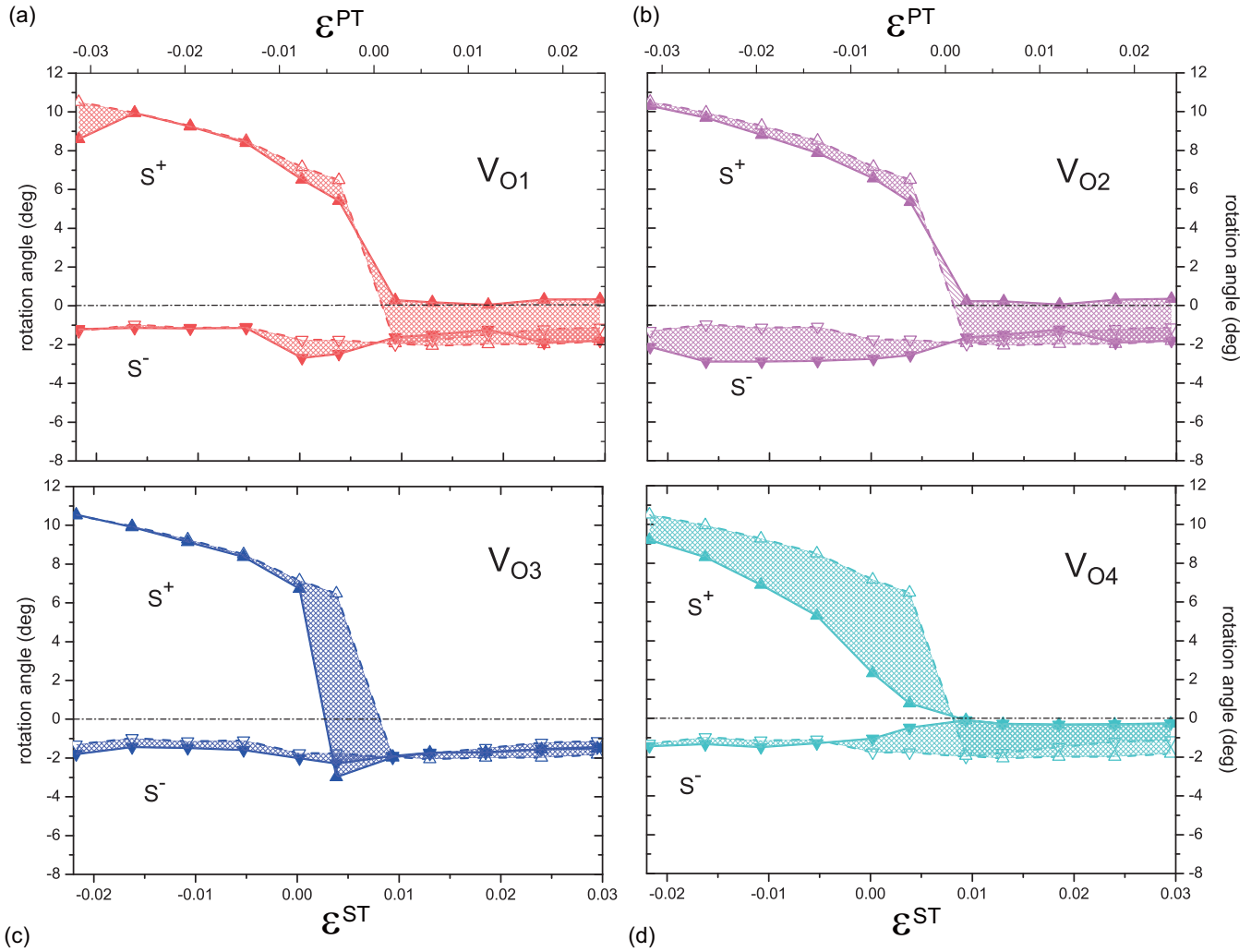
FIG. 7. (Color online) The octahedral rotations around the c axis in SL with (a) V_{O1}, (b) V_{O2}, (c) V_{O3}, and (d) V_{O4} under different epitaxial strains. The solid lines with solid symbols represent the rotations in oxygen-deficient SL, while the dashed lines with hollow symbols represent the rotations in perfect SL and the shaded areas are only for eye guidance to show the change of the rotation angles.

configurations show almost similar trends to those in perfect superlattice. Only the S^- rotation of superlattice with V_{O2} gets larger and the S^+ rotation of superlattice with V_{O4} becomes smaller compared to the perfect superlattice. As the in-plane lattice parameter increases while the condition $\varepsilon^{PT} < 0$ is also satisfied, the S^+ rotation angles in superlattices with V_{O3} and V_{O4} decrease faster than those in the perfect superlattice, revealing that the rotation around the c axis is not robust in the existence of V_{O3} and V_{O4}.

When the superlattice is further stretched to $\varepsilon^{PT} > 0$, the octahedral rotations in different configurations will result in quite different patterns. For the superlattice with V_{O1} or V_{O2}, the rotation angles in the upper layer (S^+ rotation) decrease to zero while in the lower layer (S^- rotation) are stable at 1°–2°. This inequivalence of the S^+ and S^- rotations is attributed to the incompleteness of the octahedra in one layer upon the removal of O1 or O2, and accompanied by the nonzero [001] polarizations shown in Figs. 5(a) and 5(b). On the contrary, in the superlattice with V_{O3} or V_{O4}, the rotation angles in the upper layers and lower layers converge to the same values at tensile

strain because the upper-layer and lower-layer "octahedra" are still symmetrical even though they are both defective with the lack of an oxygen atom each. In superlattices with V_{O4}, the S^+ and S^- rotation angles both decrease to almost zero. This is due to the V_{O4}-induced outward motions of Sr atoms. As a matter of fact, because the atomic interaction in the SrO plane is the driving force for the octahedral rotation, the loss of O atom in the SrO plane itself can be the reason for the reduction of the rotation around the c axis. The S^+ and S^- rotations in superlattice with V_{O3} are almost the same as those in the perfect superlattice and maintained in the range of 1.5°–2°, which is consistent with the nearly unchanged polarization in superlattice with this kind of V_O.

As for the tilts around the in-plane axes, there exist some novel features. It is shown above that, in pristine superlattice, compressive strain can suppress the in-plane tilts. The introduction of V_O, however, may cause certain lattice distortions and atomic displacements. Thus, several octahedra near V_O can have sizable in-plane tilts even under large compressive strain. We denote those tilts emerging under large compressive
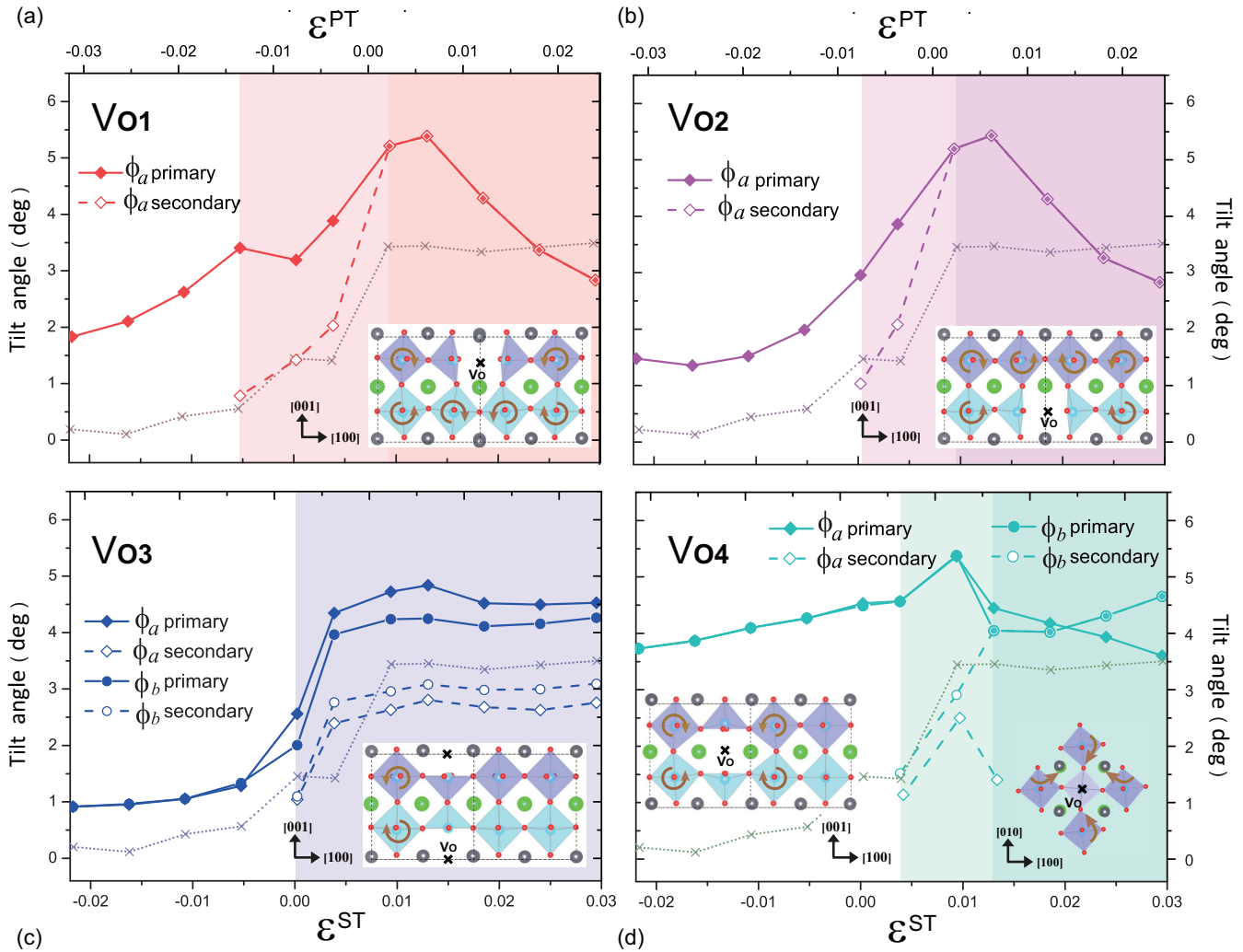
FIG. 8. (Color online) The in-plane octahedral tiltings along the [100] and [010] directions in terms of epitaxial strain for SL with (a) V_{O1}, (b) V_{O2}, (c) V_{O3}, and (d) V_{O4} in comparison with the rotation projected along the [100] direction in perfect SL (dotted lines with crosses). The light shade indicates the emergence of the secondary tilts, and the deep shade indicates that secondary tilts are as large as the primary tilts to form an overall in-plane tilt pattern. Note there is only one type of shade in (c) where the secondary tilts are always smaller than the primary tilts. The positions of octahedra with primary tilts under compressive strain are marked in the insets.

strain as primary tilts. The octahedra which have primary tilts are marked in the insets of Fig. 8. For convenience, we denote the octahedron chain with two successive imperfect octahedra (TiO_5 polyhedra) as d chain (i.e., defective octahedron chain). In other words, the d chain consists of successive octahedra along the Ti-V_O-Ti direction. From the insets of Figs. 8(a) and 8(b), the octahedra in the d chain and the octahedron chains just below or above the d chain have primary tilts in the superlattice with V_{O1} or V_{O2}. If the d chain is [010] oriented, the tilts turn to be around the [100] direction since the vacancy-induced atomic displacements along the chain cannot produce the rotation around the chain. The same rule can be applied to the [100]-oriented d chain. In contrast to V_{O1} and V_{O2} configurations, the nearest-neighboring octahedra of the TiO_5 polyhedra in superlattice with V_{O3} or V_{O4} may bear primary tilts around both the [100] and [010] axes. Only four octahedra surrounding V_{O3} have small primary tilts of about $1°$ under compressive strain, while all eight nearby octahedra surrounding V_{O4} manifest the primary tilts as large as $4°$.

After the superlattice is stretched to a certain degree (corresponding to the areas covered with lighter shades in Fig. 8), the octahedra which do not tilt at large compressive strain can now have in-plane tilts as the "secondary tilts" as shown in the insets of the figure. At around $\varepsilon^{PT} = 0$, the secondary tilts have similar magnitudes to primary tilts and an overall in-plane tilt pattern forms except for the V_{O3} configuration. In superlattices with V_{O1} or V_{O2} the tilts are still around the [100] direction only. In the V_{O4} configuration, there are tilts around both the [100] and [010] directions and the tilt angles are larger than those in perfect superlattices. Combining these results with the rotations around the c axis, it is clear that the V_O can suppress the rotations or tilts around the axis parallel to the d chain (the Ti-V_O-Ti chain), but facilitate the rotations around the other two orthogonal axes. Finally, if the tensile strain increases further, the tilt angles are slightly reduced instead of enhanced. Because the octahedra with V_O defect deform too much under large strains, the rigid oxygen cage approximation is not applicable and more types of distortions

need to be considered, which are beyond the scope of this paper.

V. DISCUSSIONS

In this section we qualitatively discuss the interplay between polarization and octahedral rotations (tilts), and the role of V_O in this coupling. As mentioned before, the S$^+$ and S$^-$ octahedra are equivalent by symmetry in undistorted PT/ST 1/1 superlattices. The nonzero polarization along the c axis can distinguish the octahedra in upper layers from those in lower layers. It is shown that the orientation of the out-of-plane polarization relates to the rotations of S$^+$ and S$^-$ octahedra in a straightforward way: the upper-layer octahedra rotate more than lower-layer octahedra when the polarization points down and vice versa, which is consistent with previous theoretical work [8]. Summarizing the polarization variations and octahedral rotations around the c axis of the FE$_r$/AFD$_{aac}$, FE$_c$/AFD$_c$, and FE$_{aa}$/AFD$_{aa}$ phases as shown in Fig. 2, we find that roughly the difference between S$^+$ rotation and S$^-$ rotation depends linearly on the out-of-plane polarization: $\mid \phi_c(\mathrm{S}^+) - \phi_c(\mathrm{S}^-) \mid \propto \mid P_c \mid$. With the introduction of oxygen vacancies, $\mid \phi_c(\mathrm{S}^+) - \phi_c(\mathrm{S}^-) \mid$ is still positively correlated with the out-of-plane polarization. Compared to the perfect one, superlattices with V_{O1} or V_{O2} still has nonzero [001] polarization of about 5 μC/cm^2 under tensile strain, corresponding to the difference of 2° in rotation angles. For V_{O4} configuration, the out-of-plane polarization is reduced to zero under tensile strain and accordingly the difference between S$^+$ rotation and S$^-$ rotation vanishes. Therefore, although the presence of oxygen vacancies can influence the magnitudes of the out-of-plane polarization and rotations around the c axis, it will not noticeably affect the positive correlation between $\mid \phi_c(\mathrm{S}^+) - \phi_c(\mathrm{S}^-) \mid$ and $\mid P_c \mid$.

In perfect superlattices, it is observed that octahedral rotation accompanies the polar distortion along the rotational axis, similar to the case in rhombohedral BiFeO$_3$ [55]. This can be regarded as a result of strain mediation. The coexistence of octahedral rotation and polar distortion is not altered by the introduction of V_O as shown by our results. The internal stress induced by V_O switches the in-plane polarization from the [110] direction to the [100] direction and simultaneously wipes out the [010] tilt, leaving only the in-plane tilt about the [100] axis. Therefore, no matter whether in perfect superlattices or oxygen-deficient superlattices the Landau expansion of total energy should have an energy-lowering term describing the coupling between polarization and rotation around the polar axis, as proposed by Bousquet *et al.* in a defect-free PT/ST 1/1 superlattice [7].

Evidently, the direction of the Ti-V_O-Ti chain is special in oxygen-deficient superlattice since the polarizations and octahedral rotations or tiltings along the chain are different from those along the other two orthogonal directions. The spontaneous polarization along the Ti-V_O-Ti chain is dramatically reduced due to the tail-to-tail polarization pattern, together with the suppressed octahedral rotation or tilting around the chain. In contrast, the polarizations only slightly decrease and octahedra rotation angles turn to increase instead of decrease in other two directions. These structural distortions are in accordance with the outward movements of neighboring

cations and inward movements of neighboring O ions. It should be noted that the changes in atomic structure will be accompanied by the modulation of the electronic structure. In particular, the V_O and epitaxial strain can synergistically affect the electronic structure around the Fermi level, including band gap and the positions of in-gap states (see the Supplemental Material [29] for a detailed analysis). It is thus that, by controlling the positions of oxygen vacancies, both the FE and AFD properties can be manipulated. In various perovskite compounds, it is possible to grow a chain or even an array of of V_O as summed up by Scott and Dawber [50] decades ago. In the same way, the polarization along a certain direction can be suppressed and the response mode can be accordingly modified in the superlattices.

VI. CONCLUSIONS

We comprehensively investigate the effect of oxygen vacancies on the FE and AFD properties of PT/ST 1/1 superlattice under different epitaxial strains. Consistent with previous work, the FE$_r$/AFD$_{aac}$ phase with space group Pc is found to be the most stable phase for the perfect superlattice, and has both in-plane and out-of-plane polarizations at intermediate strain. Interestingly, the oxygen vacancies form easiest at intermediate strain because under large tensile strain or compressive strain the polarization-induced internal electric field is stronger and can firmly bind the oxygen ions. With the presence of oxygen vacancies, the total polarizations of the superlattice tend to be pinned to the [001] direction or the in-plane direction due to the V_O-induced polarization-cancelling tail-to-tail pattern, thus inhibiting the **FE$_r$** behavior. As for the oxygen octahedral rotations around the c axis, oxygen vacancies have little influence on the rotations at large compressive strain, but lead to defect-type-dependent rotation modes at large tensile strain. In addition, oxygen vacancies can induce tilts of several octahedra around an in-plane axis at large compressive strain and subsequently an overall in-plane antiferrodistortive pattern (i.e., the in-plane tilts are promoted by oxygen vacancies).

Actually, some essential properties of PT/ST superlattices have not been altered by V_O. In both perfect and defective superlattices, octahedral rotations around the polar axis co-exist with the polarization, and the out-of-plane polarization determines the difference between the rotations in the upper layers and lower layers around the c axis. However, in the direction of the Ti-V_O-Ti chain both the polarizations and octahedral rotations are different from those along the other two orthogonal directions. The polarization in this direction is largely suppressed by the V_O-introduced tail-to-tail polarization pattern. The octahedral rotation or tilting around the Ti-V_O-Ti chain is also suppressed to some extent while the rotations or tilts at the other two directions are enhanced. As a result, the V_O-induced anisotropy in the FE and AFD properties, which may be controlled via the sample growth with oxygen vacancy chains or even planes in certain directions, can be used in the design of ferroelectric-dielectric devices. In summary, our work provides a thorough reference to the coupling of different instabilities in the oxygen-deficient superlattices and might serve as a guidance to the possible modulation means in experiments.

[1] D. G. Schlom, L. Q. Chen, C. B. Eom, K. M. Rabe, S. K. Streiffer, and J. M. Triscone, Annu. Rev. Mater. Res. **37**, 589 (2007).

[2] H. N. Lee, H. M. Christen, M. F. Chisholm, C. M. Rouleau, and D. H. Lowndes, Nature (London) **433**, 395 (2005).

[3] C. L. Hung, Y. L. Chueh, T. B. Wu, and L. J. Chou, J. Appl. Phys. **97**, 034105 (2005).

[4] J. Kim, Y. Kim, Y. S. Kim, J. Lee, L. Kim, and D. Jung, Appl. Phys. Lett. **80**, 3581 (2002).

[5] J. M. Rondinelli and N. A. Spaldin, Adv. Mater. **23**, 3363 (2011).

[6] J. B. Neaton and K. M. Rabe, Appl. Phys. Lett. **82**, 1586 (2003).

[7] E. Bousquet, M. Dawber, N. Stucki, C. Lichtensteiger, P. Hermet, S. Gariglio, J. M. Triscone, and P. Ghosez, Nature (London) **452**, 732 (2008).

[8] P. Aguado-Puente, P. Garcia-Fernandez, and J. Junquera, Phys. Rev. Lett. **107**, 217601 (2011).

[9] J. M. Rondinelli and C. J. Fennie, Adv. Mater. **24**, 1961 (2012).

[10] W. Siemons, G. Koster, H. Yamamoto, T. H. Geballe, D. H. A. Blank, and M. R. Beasley, Phys. Rev. B **76**, 155111 (2007).

[11] N. Biskup, J. Salafranca, V. Mehta, M. P. Oxley, Y. Suzuki, S. J. Pennycook, S. T. Pantelides, and M. Varela, Phys. Rev. Lett. **112**, 087202 (2014).

[12] D. D. Cuong, B. Lee, K. M. Choi, H. S. Ahn, S. Han, and J. Lee, Phys. Rev. Lett. **98**, 115503 (2007).

[13] M. Choi, F. Oba, Y. Kumagai, and I. Tanaka, Adv. Mater. **25**, 86 (2013).

[14] C. H. Park and D. J. Chadi, Phys. Rev. B **57**, R13961 (1998).

[15] C. Ederer and N. A. Spaldin, Phys. Rev. B **71**, 224103 (2005).

[16] X. F. Wu, K. M. Rabe, and D. Vanderbilt, Phys. Rev. B **83**, 020104 (2011).

[17] P. Zubko, N. Jecklin, A. Torres-Pardo, P. Aguado-Puente, A. Gloter, C. Lichtensteiger, J. Junquera, O. Stephan, and J. M. Triscone, Nano Lett. **12**, 2846 (2012).

[18] M. Dawber, N. Stucki, C. Lichtensteiger, S. Gariglio, P. Ghosez, and J. M. Triscone, Adv. Mater. **19**, 4153 (2007).

[19] P. Aguado-Puente and J. Junquera, Phys. Rev. B **85**, 184105 (2012).

[20] J. L. Blok, D. H. A. Blank, G. Rijnders, K. M. Rabe, and D. Vanderbilt, Phys. Rev. B **84**, 205413 (2011).

[21] F. Bern, M. Ziese, A. Setzer, E. Pippel, D. Hesse, and I. Vrejoiu, J. Phys.: Condens. Matter **25**, 496003 (2013).

[22] N. Al-Aqtash, A. Alsaad, and R. Sabirianov, J. Appl. Phys. **116**, 074112 (2014).

[23] S. Hao, G. Zhou, X. Wang, J. Wu, W. Duan, and B.-L. Gu, Appl. Phys. Lett. **86**, 232903 (2005).

[24] N. D. Huang, Z. R. Liu, Z. Q. Wu, J. Wu, W. H. Duan, B. L. Gu, and X. W. Zhang, Phys. Rev. Lett. **91**, 067602 (2003).

[25] G. Kresse and J. Furthmüller, Phys. Rev. B **54**, 11169 (1996).

[26] P. E. Blöchl, Phys. Rev. B **50**, 17953 (1994).

[27] P. Hohenberg and W. Kohn, Phys. Rev. **136**, B864 (1964).

[28] W. H. Press, *Numerical Recipes: The Art of Scientific Computing*, 3rd ed. (Cambridge University Press, Cambridge, UK, 2007).

[29] See Supplemental Material at http://link.aps.org/supplemental/10.1103/PhysRevB.92.115435 for details of the band structures of perfect and oxygen-deficient $PbTiO_3/SrTiO_3$ superlattices.

[30] W. Luo, W. Duan, S. G. Louie, and M. L. Cohen, Phys. Rev. B **70**, 214109 (2004).

[31] Z. Alahmed and H. Fu, Phys. Rev. B **76**, 224101 (2007).

[32] J. Bang, Z. Li, Y. Y. Sun, A. Samanta, Y. Y. Zhang, W. Zhang, L. Wang, X. Chen, X. Ma, Q.-K. Xue *et al.*, Phys. Rev. B **87**, 220503 (2013).

[33] R. Resta, Rev. Mod. Phys. **66**, 899 (1994).

[34] B. Meyer and D. Vanderbilt, Phys. Rev. B **65**, 104111 (2002).

[35] M. Gajdoš, K. Hummer, G. Kresse, J. Furthmüller, and F. Bechstedt, Phys. Rev. B **73**, 045112 (2006).

[36] Y. Yao and H. Fu, Phys. Rev. B **84**, 064112 (2011).

[37] T. Shimada, T. Ueda, J. Wang, and T. Kitamura, Phys. Rev. B **87**, 174111 (2013).

[38] Actually, it is unreasonable to decompose the polarization to a single PbO layer or SrO layer for two reasons. First, the layer polarizations are defined in two-dimensional atomic layers and have the unit of dipole moment per unit area. To transform this unit to the correct unit of polarization (dipole moment per unit volume), layer polarizations have to be divided by the distance between two neighboring layers, which still requires the positions of both the Pb(Sr)O layer and the TiO layer. Secondly and more importantly, in our scheme of polarization calculation, i.e., the widely used method of Meyer and Vanderbilt, the sum of Born effective charges in a single Pb(Sr)O layer or TiO layer does not necessarily vanish, and thus the definition of layer polarization fails [X. Wu, O. Diéguez, K. M. Rabe, and D. Vanderbilt, Phys. Rev. Lett. **97**, 107602 (2006)]..

[39] A. M. Glazer, Acta Crystallogr., Sect. B **28**, 3384 (1972).

[40] N.-H. Chan, R. Sharma, and D. M. Smyth, J. Electrochem. Soc. **128**, 1762 (1981).

[41] C. Mitra, C. Lin, J. Robertson, and A. A. Demkov, Phys. Rev. B **86**, 155105 (2012).

[42] J. Carrasco, F. Illas, N. Lopez, E. A. Kotomin, Y. F. Zhukovskii, R. A. Evarestov, Y. A. Mastrikov, S. Piskunov, and J. Maier, Phys. Rev. B **73**, 064106 (2006).

[43] R. Evarestov, E. Kotomin, and Y. F. Zhukovskii, Int. J. Quantum Chem. **106**, 2173 (2006).

[44] X. Z. Lu, X. G. Gong, and H. J. Xiang, Comput. Mater. Sci. **91**, 310 (2014).

[45] N. A. Pertsev, A. G. Zembilgotov, and A. K. Tagantsev, Phys. Rev. Lett. **80**, 1988 (1998).

[46] Note that "r phase" here does not mean that the structure is in rhombohedral phase. Instead, the structure is actually in monoclinic phase. We borrow the saying of "r phase" from Ref. [45] in which the thin film ferroelectric state $P_1 = P_2 \neq 0$, $P_3 \neq 0$ was denoted as the "r phase."

[47] J. P. Buban, H. Iddir, and S. Ogut, Phys. Rev. B **69**, 180102 (2004).

[48] L. X. He and D. Vanderbilt, Phys. Rev. B **68**, 134103 (2003).

[49] N. Wang, D. West, J. Liu, J. Li, Q. Yan, B.-L. Gu, S. B. Zhang, and W. Duan, Phys. Rev. B **89**, 045142 (2014).

[50] J. F. Scott and M. Dawber, Appl. Phys. Lett. **76**, 3801 (2000).

[51] M. Dawber and J. F. Scott, Appl. Phys. Lett. **76**, 1060 (2000).

[52] A. K. Tagantsev, I. Stolichnov, E. L. Colla, and N. Setter, J. Appl. Phys. **90**, 1387 (2001).

[53] M. L. Li, Y. J. Gu, Y. Wang, L. Q. Chen, and W. H. Duan, Phys. Rev. B **90**, 054106 (2014).

[54] P. Ghosez, J. P. Michenaud, and X. Gonze, Phys. Rev. B **58**, 6224 (1998).

[55] C. Ederer and N. A. Spaldin, Phys. Rev. B **71**, 060401 (2005).